Circumpolar Arctic Tundra Vegetation Change Is Linked to Sea Ice Decline

Uma S. Bhatt*,+ Donald A. Walker,# Martha K. Raynolds,# Josefino C. Comiso,@ Howard E. Epstein,& Gensuo Jia, Rudiger Gens,++ Jorge E. Pinzon,## Compton J. Tucker,## Craig E. Tweedie,@@ and Patrick J. Webber&&**

+Geophysical Institute, and Department of Atmospheric Sciences, University of Alaska Fairbanks, Fairbanks, Alaska
#Institute of Arctic Biology, and Department of Biology and Wildlife, University of Alaska Fairbanks, Fairbanks, Alaska
@Cryospheric Sciences Branch, NASA Goddard Space Flight Center, Greenbelt, Maryland
&Department of Environmental Sciences, University of Virginia, Charlottesville, Virginia
**RCE-TEA, Institute of Atmospheric Physics, Beijing, China
++Geophysical Institute, and Alaska Satellite Facility, University of Alaska Fairbanks, Fairbanks, Alaska
##Biospheric Science Branch, NASA Goddard Space Flight Center, Greenbelt, Maryland
@@Department of Biology, University of Texas at El Paso, El Paso, Texas
&&Department of Plant Biology, Michigan State University, East Lansing, Michigan

Received 7 December 2009; accepted 4 May 2010

ABSTRACT: Linkages between diminishing Arctic sea ice and changes in Arctic terrestrial ecosystems have not been previously demonstrated. Here, the authors use a newly available Arctic Normalized Difference Vegetation Index (NDVI) dataset (a measure of vegetation photosynthetic capacity) to document coherent temporal relationships between near-coastal sea ice, summer tundra land surface temperatures, and vegetation productivity. The authors find that,

* Corresponding author address: Uma S. Bhatt, Geophysical Institute, and Department of Atmospheric Sciences, University of Alaska Fairbanks, 930 Koyukuk Drive, Fairbanks, AK, 99775.
E-mail address: usbhatt@alaska.edu

DOI: 10.1175/2010EI315.1

during the period of satellite observations (1982–2008), sea ice within 50 km of the coast during the period of early summer ice breakup declined an average of 25% for the Arctic as a whole, with much larger changes in the East Siberian Sea to Chukchi Sea sectors (>44% decline). The changes in sea ice conditions are most directly relevant and have the strongest effect on the villages and ecosystems immediately adjacent to the coast, but the terrestrial effects of sea ice changes also extend far inland. Low-elevation (<300 m) tundra summer land temperatures, as indicated by the summer warmth index (SWI; sum of the monthly-mean temperatures above freezing, expressed as °C month^{-1}), have increased an average of 5°C month^{-1} (24% increase) for the Arctic as a whole; the largest changes (+10° to 12°C month^{-1}) have been over land along the Chukchi and Bering Seas. The land warming has been more pronounced in North America (+30%) than in Eurasia (16%). When expressed as percentage change, land areas in the High Arctic in the vicinity of the Greenland Sea, Baffin Bay, and Davis Strait have experienced the largest changes (>70%). The NDVI has increased across most of the Arctic, with some exceptions over land regions along the Bering and west Chukchi Seas. The greatest change in absolute maximum NDVI occurred over tundra in northern Alaska on the Beaufort Sea coast [+0.08 Advanced Very High Resolution Radiometer (AVHRR) NDVI units]. When expressed as percentage change, large NDVI changes (10%–15%) occurred over land in the North America High Arctic and along the Beaufort Sea. Ground observations along an 1800-km climate transect in North America support the strong correlations between satellite NDVI observations and summer land temperatures. Other new observations from near the Lewis Glacier, Baffin Island, Canada, document rapid vegetation changes along the margins of large retreating glaciers and may be partly responsible for the large NDVI changes observed in northern Canada and Greenland. The ongoing changes to plant productivity will affect many aspects of Arctic systems, including changes to active-layer depths, permafrost, biodiversity, wildlife, and human use of these regions. Ecosystems that are presently adjacent to year-round (perennial) sea ice are likely to experience the greatest changes.

KEYWORDS: Arctic climate; Sea ice; Tundra vegetation

1. Introduction

Arctic land surface temperatures have increased (Kaufman et al. 2009) and are predicted to continue warming with major repercussions for terrestrial ecosystems (ACIA 2004; Serreze et al. 2007; Post et al. 2009). Observational studies have documented the well-known cooling effect that sea ice has on adjacent landmasses (Rouse 1991; Haugen and Brown 1980), whereas global climate model simulations show that coastal Arctic land surfaces warm when summer sea ice decreases (Bhatt et al. 2008; Lawrence et al. 2008). We might also expect a strong linkage between sea ice concentrations and tundra productivity, because approximately 80% of non-alpine tundra is located within 100 km of a coastline, making it essentially a maritime biome (Walker et al. 2005). However, the direct observational linkages between sea ice retreat, land warming, and increased terrestrial productivity have not heretofore been established. Here we examine the hypothesis that the decline in sea ice is linked to increases in land temperatures and tundra productivity. We use a newly available satellite-derived dataset of Arctic Normalized Difference Vegetation Index (NDVI; J. E. Pinzon et al. 2010, unpublished manuscript) to demonstrate a

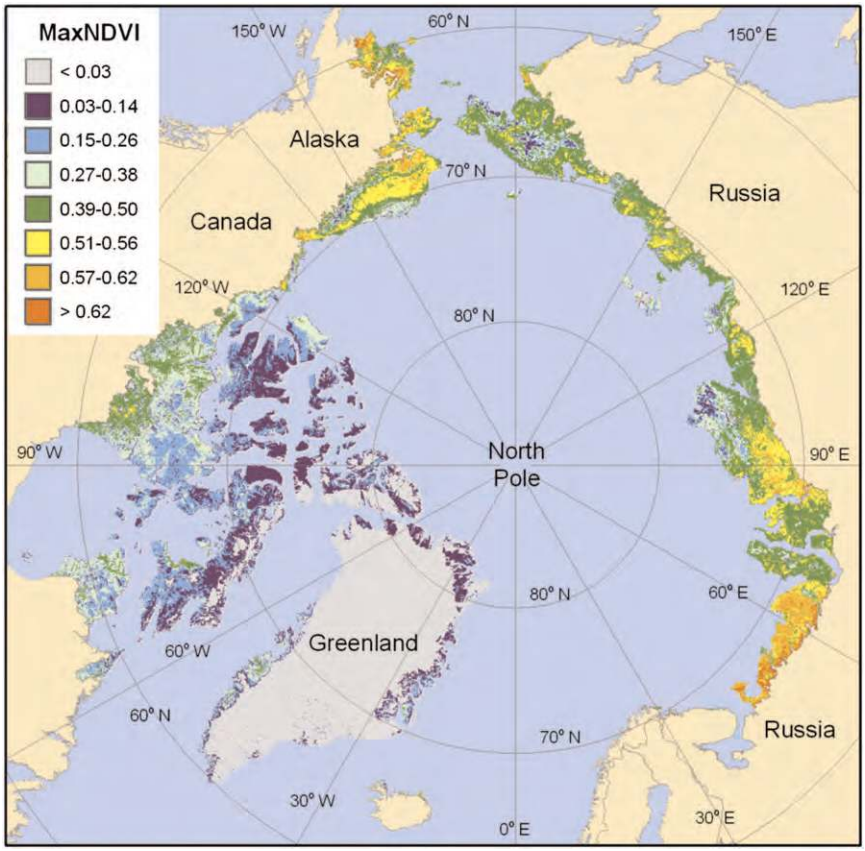

Figure 1. Circumpolar maximum NDVI of Arctic tundra. This image is a mosaic of AVHRR data portraying the maximum NDVI for each pixel during the summers of 1993 and 1995, 2 years of relatively low summer cloud cover in the High Arctic (Walker et al. 2005). Areas of high NDVI (oranges and reds) correspond to regions of dense shrub cover. Yellow and green areas generally have peaty soil surface horizons and are continuously vegetated with mosses, sedges, and dwarf shrubs. Light green areas approximately correspond to areas of incomplete vegetation cover, often comprised of prostrate dwarf shrubs. Low NDVI (blues) corresponds to areas with sparse, very-low-growing plant cover on mineral soils, such as high mountains and much of the High Arctic.

consistent temporal relationship between sea ice, NDVI, and land temperatures over Arctic tundra. These data permitted the first circumpolar analysis over tundra of NDVI changes in the High Arctic north of 72°N.

The spatial patterns of NDVI are most strongly related to land temperatures and the glacial history of the landscapes (Raynolds et al. 2010, manuscript submitted to *Ecography*). The circumpolar pattern of average annual maximum NDVI (MaxNDVI; Figure 1) corresponds also to nearby sea ice cover, with the lowest MaxNDVI values in the Canadian Archipelago, northern Greenland, and other Arctic islands adjacent to the perennial sea ice. The presence of the near-shore

summer sea ice limits the ability of the land surface to warm during the summer. The photosynthetic capacity of Arctic vegetation, as measured from satellites using the NDVI, has increased over the last 25+ years (Jia et al. 2003; Goetz et al. 2005; Bunn et al. 2007; Verbyla 2008). This trend has been attributed to an increase in shrubs (Tape et al. 2006; Lantz 2008) and a longer growing season (Jia et al. 2003). There have also been notable declines of summer sea ice area (Comiso et al. 2008), extent (Stroeve et al. 2008), and thickness during the past several decades (Rothrock et al. 2008; Kwok and Rothrock 2009). Mean annual surface air temperatures based on pan-Arctic station data poleward of 60°N have increased 1.4°C over the last century with the most rapid warming documented at maritime stations adjacent to areas of declining sea ice (Bekryaev et al. 2010).

2. Data and methods

This study used estimates of sea ice concentration from Special Sensor Microwave Imager (SSM/I) data (Comiso and Nishio 2008) and Advanced Very High Resolution Radiometer (AVHRR) radiometric surface temperature from 1982 to 2008. The surface temperature data have been enhanced through more effective cloud masking techniques and calibration through the utilization of in situ surface temperature data (Comiso 2003). The summer warmth index (SWI) was calculated as the sum of average May–September monthly surface temperatures above freezing at each pixel.

The NDVI represents the fraction of photosynthetically active radiation (fPAR) that is absorbed by the plant canopy and depends on a variety of vegetation properties such as vertical and horizontal structure, species composition, phenological stage, and physiological condition. The NDVI has been used extensively to monitor vegetation changes in the Arctic (Stow et al. 2004). The reflectivity of green plants varies with wavelength, which is the basis for the NDVI index: NDVI = (NIR − RED)/(NIR + RED), where NIR is surface reflectance in the near infrared (0.725–1.1 μm) and RED is the reflectance in the visible radiation (0.55–0.70 μm).

Remotely sensed 8-km-resolution National Aeronautics and Space Administration (NASA) Global Inventory Modeling and Mapping Studies (GIMMS; available online at http://gimms.gsfc.nasa.gov/) biweekly maximum NDVI data (J. E. Pinzon et al. 2010, unpublished manuscript) are derived from AVHRR sensors that were flown on *National Oceanic and Atmospheric Administration-7* (*NOAA-7*) through *NOAA-18* satellites. This new dataset corrected discontinuities in the GIMMS NDVI north of 72°N and permitted the first comprehensive analysis of NDVI trends in the High Arctic. The new GIMMSg3 dataset uses the Sea-Viewing Wide-Field-of-View Sensor (SeaWiFS) for calibrating between sensors. The old GIMMS series used SPOT data, which only had coverage to 72°N and created an artificial boundary at that latitude. The AVHRR time series was compared with data from Moderate Resolution Imaging Spectroradiometer (MODIS), which samples narrower wavelengths and produces an NDVI that is considered more accurate than the AVHRR NDVI. The AHVRR data for the period of overlapping coverage show the same trends and variability as the MODIS data, validating the accuracy and consistency of the AVHRR time series. This study used approximately 12-km-resolution NDVI data to more closely match the other observations. The MaxNDVI is the highest summer NDVI value, representing peak

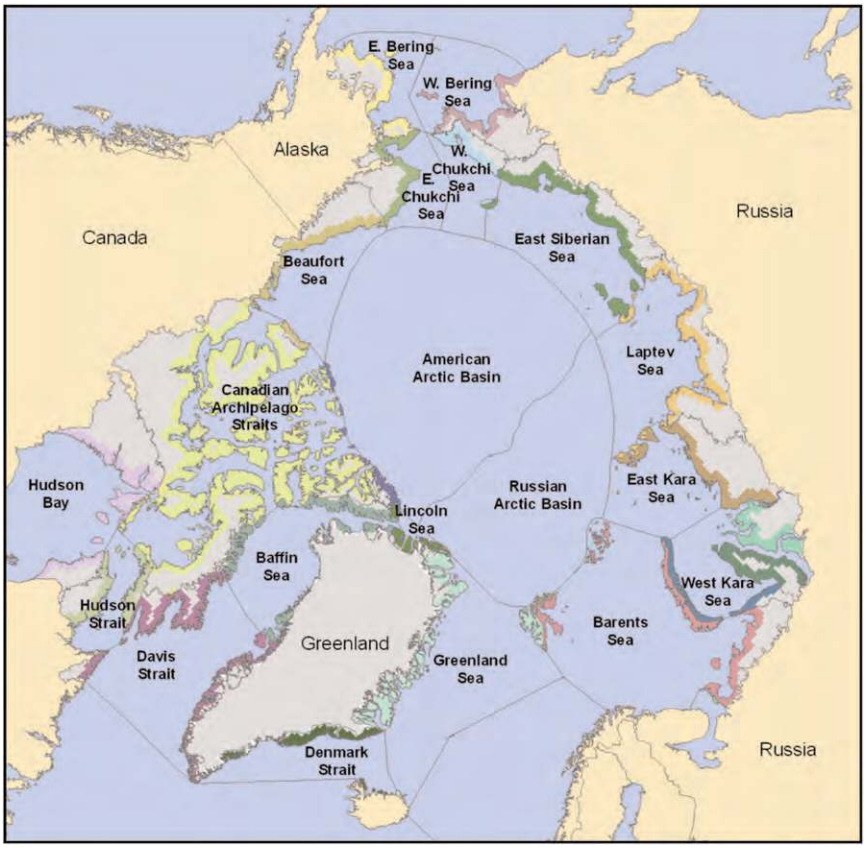

Figure 2. Map identifying oceanic and terrestrial regions of the Arctic used in the analysis. Color over land is used to help differentiate between the tundra regions.

vegetation photosynthetic capacity, and serves as an indicator of tundra biomass (Shippert et al. 1995; Walker et al. 2003). The unitless time-integrated NDVI (TI-NDVI) is the sum of biweekly values above 0.05 from May to September. TI-NDVI incorporates the length of the growing season and phenological variations and better represents gross primary production than MaxNDVI (Tucker and Sellers 1986). The Arctic tundra zone was defined according to the circumpolar Arctic vegetation map (Walker et al. 2005), with a southern boundary defined by the Arctic tree line.

The Arctic Ocean was divided into subregions (Figure 2) modified from the map ''The Arctic Ocean within accepted boundaries'' in the *Arctic Atlas* (Treshnikov 1985), and the adjacent land divisions approximately follow the floristic provinces of the circumpolar Arctic vegetation map (Walker et al. 2005). For simplicity, both land and ocean areas will be identified by the name of the corresponding sea in the rest of the paper. The analysis constructs time series averaged over regions within 50 km of the Arctic coastline to focus on the domain of maximum maritime influence [approximately 60% of Arctic tundra with elevations less than 300 m is within 50 km of the coastline]. The analysis was repeated for a 100-km coastal zone and also for the full Arctic tundra region below elevations of 300 m. The

Table 1. Correlations between linearly detrended sea ice, SWI and TI-NDVI time series from 1982 to 2008, for different Pan-Arctic regions in the 50-km coastal land and ocean domains. Correlations between sea ice within 50 km of the coast and the full tundra domain are shown in parenthesis.

	Avg 50% ice concentration	Sea ice and SWI	SWI and TI-NDVI	Sea ice and TI-NDVI
Northern Hemisphere	16–22 Jul	−0.49* (−0.32)	0.64* (0.57*)	−0.56* (−0.55*)
North America	23–29 Jul	−0.56* (−0.40*)	0.60* (0.57*)	−0.53* (−0.50*)
Eurasia	9–15 Jul	−0.58* (−0.40*)	0.67* (0.65*)	−0.51* (−0.41*)
East Bering Sea	30 Apr–6 May	−0.12 (−0.04)	0.57* (0.48*)	−0.47* (−0.47*)
East Chukchi Sea	11–17 Jul	−0.13 (−0.02)	0.55* (0.51*)	−0.41* (−0.37)
Beaufort Sea	9–15 Jul	−0.37** (−0.31)	0.50* (0.31)	−0.20 (−0.17)
Canadian Archipelago	6–12 Aug	−0.77* (−0.66*)	0.78* (0.76*)	−0.64* (−0.65*)
Baffin Bay	2–8 Jul	−0.38* (−0.46*)	0.55* (0.44*)	−0.35** (−0.37**)
Davis Strait	21–27 May	0.05 (−0.19)	0.35** (0.35**)	−0.27 (−0.26)
Greenland Sea	30 Jul–5 Aug	−0.46* (−0.54*)	0.29 (0.12)	−0.17 (−0.16)
Barents Sea	21–27May	−0.50* (−0.44*)	0.65* (0.45*)	−0.34** (−0.33**)
West Kara Sea	16–22 Jul	−0.41* (−0.36)	0.56* (0.54*)	−0.28 (−0.24)
East Kara Sea	13–19 Aug	−0.41* (−0.30)	0.78* (0.74*)	−0.46* (−0.43*)
Laptev	23–29 Jul	−0.68* (−0.59*)	0.74* (0.76*)	−0.69* (−0.61*)
East Siberian Sea	23–29 Jul	−0.62* (−0.53*)	0.60* (0.62*)	−0.64* (−0.63*)
West Chukchi Sea	2–8 Jul	−0.54* (−0.49*)	0.52* (0.45*)	−0.36** (−0.32**)
West Bering Sea	14–20 May	−0.09 (−0.05)	0.39* (0.13)	0.16 (0.14)

* Significance at the 95% or greater level.
** Significance at the 90% or greater level.

results of the three analyses were similar; we report the results only for the 50-km domain, except in Table 1, where correlations over the full tundra are included. Time series of regional sea ice concentration, SWI, and NDVI were constructed for the 50-km-wide domains for the Pan-Arctic, North America, Eurasia, and Arctic subregions. The timing of the mean 50% ice concentration was most strongly correlated with SWI in the following summer and displayed high variability, so it was chosen as the base period for analyzing the sea ice data in the context of tundra vegetation. Sea ice time series were constructed using ice concentration data averaged over a 3-week period centered on the week when mean concentrations were 50%, the timing of which varied regionally (Table 1). The 60% sea ice concentration level was used for the Canadian Archipelago because a higher threshold was needed because a 50% sea ice concentration is not common in this domain. The results from the Lincoln Sea, American Arctic Basin, and Russian Arctic Basin areas were not presented because the corresponding land area was so small. Standard linear correlations and least squares fit trend lines were calculated to investigate the relationship between sea ice, NDVI, and SWI. All time series were linearly detrended before calculating correlations to separate variability and trend relationships. The statistical significance of correlations and trends was assessed using a two-tailed t test at the 5% and 10% levels.

3. Results

During our study period (1982–2008), springtime sea ice decreased in most of the Arctic (Figures 3a and 4a). Northern Hemisphere sea ice within 50 km of the coast displayed an absolute decline of 15% (Figure 5a) and a relative decline of

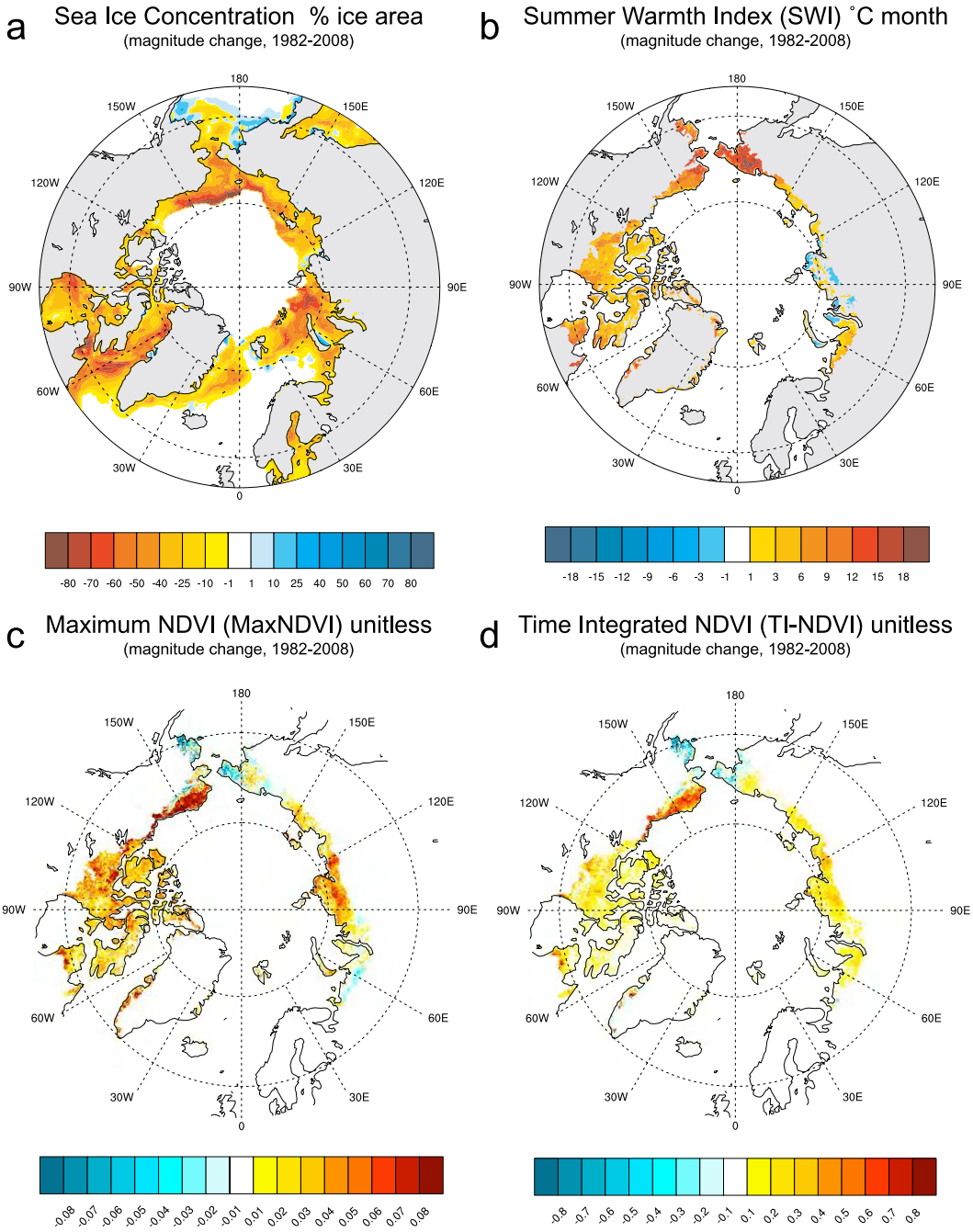

Figure 3. Magnitude of Arctic trend from 1982 to 2008 (i.e., total trend magnitude over 27 yr) of (a) sea ice concentration at the 50% climatological value, (b) SWI, (c) MaxNDVI, and (d) TI-NDVI. SWI and NDVI trends are shown only for tundra regions (southernmost plot latitude is 55°N and color scales are not linear).

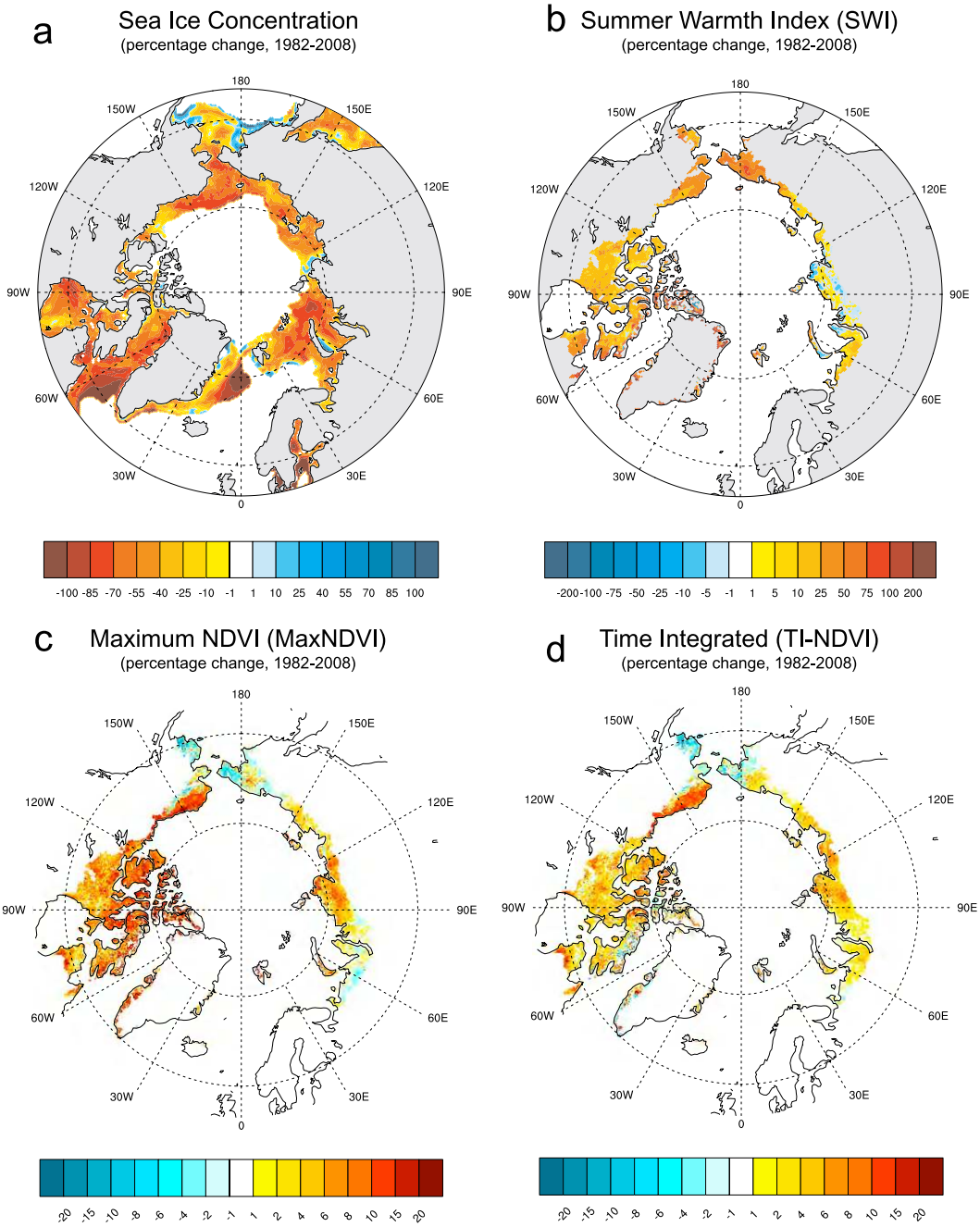

Figure 4. Percentage change in the Arctic from 1982 to 2008 (i.e., change in 27-yr trend expressed as a percent of 1982 value) of (a) sea ice concentration at the 50% climatological value, (b) SWI, (c) MaxNDVI, and (d) TI-NDVI. SWI and NDVI trends are shown only for tundra regions (southernmost plot latitude is 55°N and color scales are not linear).

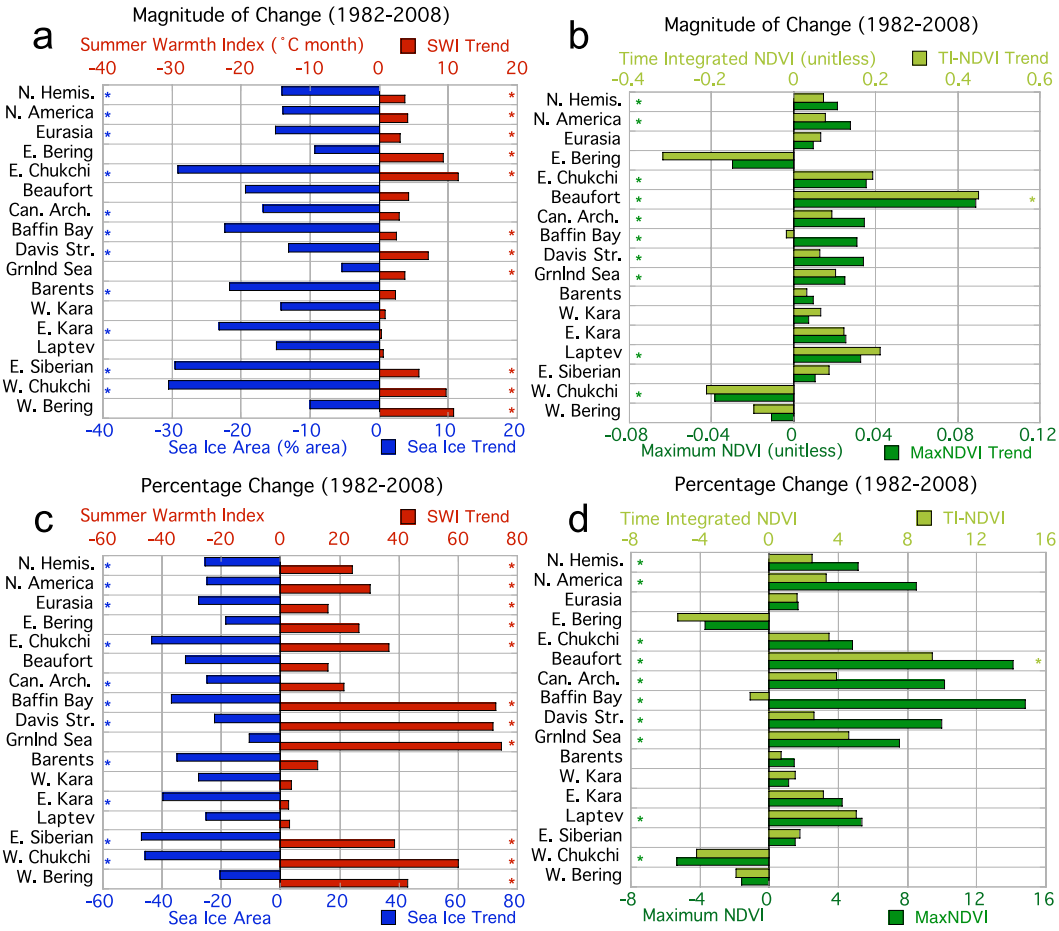

Figure 5. Magnitude of trend for different 50-km coastal zones of the Arctic from 1982 to 2008 of (a) sea ice concentration (blue) and SWI (red) and (b) MaxNDVI (dark green) and TI NDVI (light green). Percentage change for different 50-km coastal zones of the Arctic from 1982 to 2008 of (c) sea ice concentration (blue) and SWI (red) and (d) MaxNDVI (dark green) and TI-NDVI (light green). Statistically significant trends at the 95% or greater level are identified by colored stars.

25% from 1982 to 2008 (Figure 5c). The largest percentage (relative) changes of sea ice area were in the East Siberian (−47%), west Chukchi (−46%), east Chukchi (−44%), and east Kara (−40%) Seas (Figure 5c). Positive sea ice trends in a few areas such as southeast Novaya Zemlya (Figures 3a and 4a) were likely caused by an accumulation of fragmented sea ice. Sea ice in the Greenland Sea, which displayed the smallest percentage change (−10%; Figure 5c), is replenished from the Arctic through Fram Strait.

The largest absolute increases in summer land temperature were found in the Bering and Chukchi regions (>10°C month^{-1}; Figures 3b and 5a). When expressed as percentage change the summer warmth index (SWI; the sum of monthly-mean temperatures > 0°C) increased an average of 24% for the Arctic as

a whole (Figures 5c and 7a). Greater warming occurred in North America (30%) than in Eurasia (16%; Figures 5c and 7b,c). Warming trends in the vicinity of the Greenland Sea, Baffin Bay, and Davis Strait displayed the largest percentage changes (>70%; Figures 5c and 9e–g) but had relatively small magnitudes (Figure 5a). Large percentage changes in the SWI (Figure 5c) also occurred in the Beringia region (60% for west Chukchi Sea, 43% for west Bering Sea, 38% for East Siberian Sea, and 37% for east Chukchi Sea). Southern Novaya Zemlya and the northern tip of the Taimyr Peninsula, Russia, cooled, consistent with nearby coastal sea ice increases (Figures 3b and 4b). Northern Yamal, Gydan, and the southern tundra on the Taimyr also displayed cooling trends but did not have local ice decreases.

The magnitude and percentage changes in NDVI since 1982 present a generally consistent picture of increased vegetation photosynthesis in areas of land warming and sea ice decline (Figures 3c,d and 4c,d). MaxNDVI increased the most in northern Alaska, northern Canadian mainland, southwest Greenland, and Taimyr (Figure 3c). When expressed as percentage change, large increases also occurred in High Arctic Canada and Greenland (+10% for Canadian Archipelago, 5% for Baffin Bay, 10% for Davis Strait, and 8% for Greenland Sea; Figure 5d). There were declines in the Kara and Barents Seas, which displayed generally weak summer land-temperature increases. The TI-NDVI trends (Figures 5b,d) were of the same sign as MaxNDVI in all of the regions but Baffin Bay. In regions adjacent to the east Bering and west Chukchi, MaxNDVI declined (−4% and −5%, respectively) but SWI increased (27% and 60%, respectively; Figure 5d). The Bering Sea is one of few areas in the Arctic where the trends in sea ice area have been positive (Comiso and Nishio 2008), indicating a possible delay in spring greenup and a change in seasonality that is reflected in the NDVI trends.

Correlation analysis using linearly detrended time series showed that, when sea ice was below average, SWI and TI-NDVI were above normal (Figure 6), consistent with previous trends documenting strong circumpolar NDVI–surface temperature relationships (Raynolds et al. 2008). Correlations between TI-NDVI and SWI were generally high, with a 0.64 correlation for the Northern Hemisphere (Table 1). Sea ice had somewhat lower correlations with SWI (−0.49 for the Northern Hemisphere) and TI-NDVI (−0.56). Because the NDVI and SWI are collocated and integrated measures, it is expected that these correlations would be higher than those with sea ice. Springtime sea ice and summer land temperatures are significantly correlated in 9 of 14 Arctic sea regions, land temperatures and NDVI are significantly correlated in 12, and sea ice and NDVI are significantly correlated in 6 (Table 1). When TI-NDVI and SWI were calculated using the full tundra domain, the correlations with sea ice were generally slightly weaker but still strongly significant (Table 1).

Time series from 1982 to 2008 of sea ice concentration (blue), SWI (red), MaxNDVI (dark green), and TI-NDVI (light green), displayed for the hemispheric, Eurasian, and North American domains (Figures 7–9), indicate that interannual variability is overall larger in the Eurasian seas. However, east Bering, east Chukchi, and Beaufort Seas (Figures 9a–c) display the largest standard deviations in individual seas for SWI and sea ice concentration ranging from 3.9° to 4.2°C month^{-1} and from 17.9% to 19.7%, respectively. The variability in the Canadian Arctic (Figures 9d–f) is generally low for all variables, contributing to the smaller variance in North America versus Eurasia. Variability of MaxNDVI (TI-NDVI) is

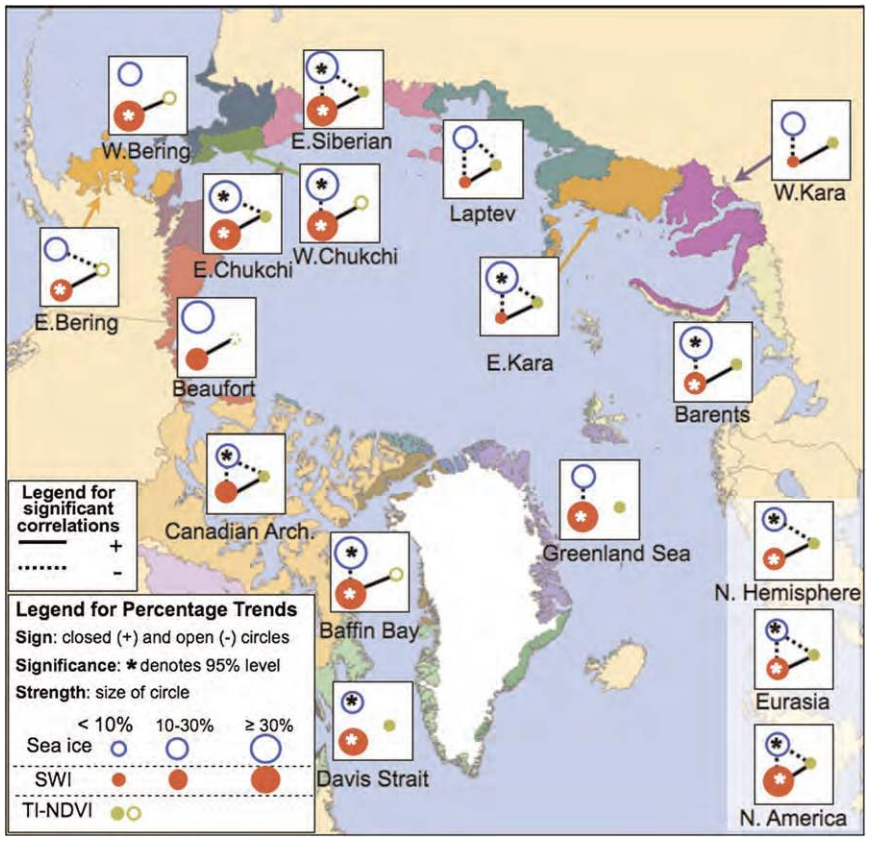

Figure 6. Regional trends and correlations between Arctic sea ice concentration (blue), SWI (red), and TI-NDVI (green) displayed as percentage change from 1982 to 2008. Strengths of trends are signified by the size of the circles. Significant linear correlation coefficients (>95%) are identified by lines that connect the trend circles. Negative trends and correlations are shown as open circles or dashed lines, respectively.

notably larger in Eurasia (Figures 7 and 8), ranging from 0.016 to 0.032 (0.140 to 0.229) compared to North America (Figures 7 and 9), where it ranges from 0.012 to 0.022 (0.088 to 0.254). The strongest correlations (Table 1) between springtime sea ice concentration and SWI are found for the Canadian Archipelago (−0.77; Figure 9d) and the Laptev regions (−0.68; Figure 8d) and are confirmed visually by strong covariability seen in the corresponding time series. These time series reinforce the notion that sea ice concentration, SWI, and NDVI vary in unison throughout the Arctic.

A few ground-based studies were available to support the conclusions of this study. The strong linkages between SWI, NDVI, and above-ground plant biomass were documented in a study of zonal vegetation along the full Arctic climate gradient in North America (Figure 10a). SWI increased from 4° to 31°C month^{-1} along the north–south temperature gradient; the corresponding NDVI (determined with hand-held instruments) of zonal vegetation increased from 0.15 to 0.52

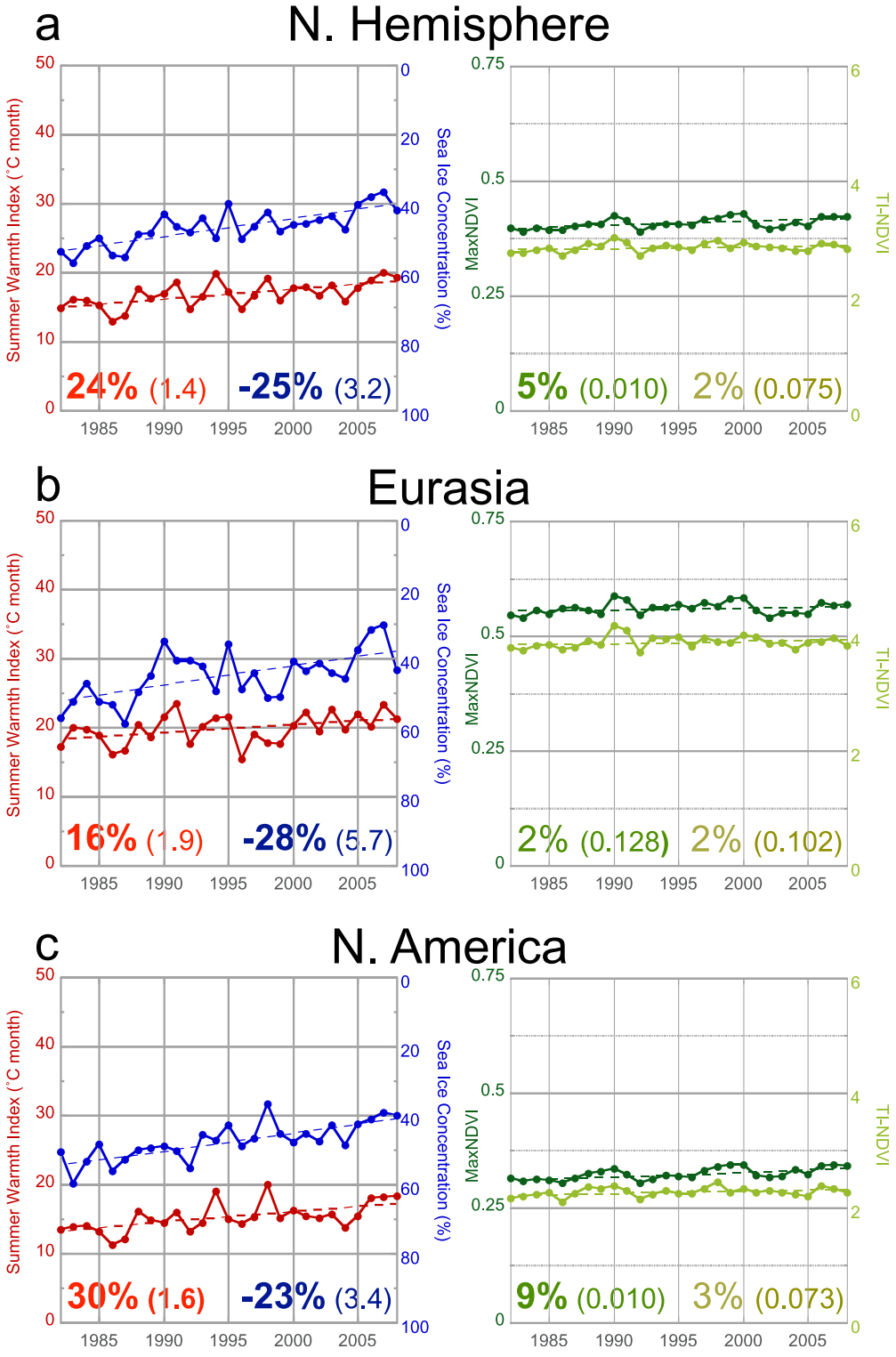
a
N. Hemisphere
Summer Warmth Index (°C month)
Sea Ice Concentration (%)
MaxNDVI
TI-NDVI
24% (1.4)
-25% (3.2)
5% (0.010)
2% (0.075)
b
Eurasia
16% (1.9)
-28% (5.7)
2% (0.128)
2% (0.102)
c
N. America
30% (1.6)
-23% (3.4)
9% (0.010)
3% (0.073)
1985
1990
1995
2000
2005

(Figure 10c), and biomass increased from 50 to 920 g m^{-2} (Figure 10d; Epstein et al. 2008). A recent 27-yr study from the Alexandra Fjord region of Ellesmere Island was the first plot-based study to document long-term tundra biomass increases in the Arctic (Hudson and Henry 2009). The study linked increases in bryophyte and evergreen shrub biomass to regional warming during the past 30–50 years. At another High Arctic site on northern Baffin Island, repeat photographs taken 46 years after the initial observations (Webber 1971) document the dramatic changes associated with vegetation succession in areas deglaciated within the past 500 years (Figure 11). The rapid revegetation of these recently exposed landscapes and the known relationship between NDVI and glacial surface age (Raynolds and Walker 2009) could help explain the very large percentage changes in MaxNDVI observed in areas adjacent to the Greenland Sea, Baffin Bay, and Davis Strait (Figure 5d), which are all areas with large retreating glaciers.

There is particularly strong potential for rapid change in the extreme High Arctic (bioclimate subzone A; Figure 10a,b), where summer-long sea ice at the coast maintains the currently very cold summer land temperatures (mean July temperatures are <3°C). These areas correspond to the ''polar desert'' described in Russian approaches to Arctic vegetation zonation (Alexandrova 1980) and have unique tundra with only about 50 Arctic vascular plant species in local floras, no woody plants, no sedges, and no *Sphagnum* mosses, and there is no peat in the wetlands. The vegetation is instead dominated by mosses; lichens; blue-green algae; and a few grasses, rushes, and forbs (Figure 10b). The vegetation is sparse here because summer temperatures are close to the biological limit for plant growth. Small increases in plant biomass, as reflected in the magnitude of the MaxNDVI, correspond to high percentage changes with large biological implications (Myers and Pitelka 1979; cf. High Arctic Canada in Figures 5b,d). Melting the summer coastal ice in subzone A will result in very large relative increases in summer land temperatures. A shift in the mean July temperature of only 2°C would likely transform the vegetation of bioclimate subzone A into something more closely resembling the vegetation of subzone B, with a potential doubling of the number of vascular plants (50–100 versus <50 species), the introduction of common tundra plant functional types that are missing in subzone A (i.e., sedges and woody plants), and a large increase in plant production from the current <30 to 50–200 g m^{-2}. There would also be major repercussions to other components of the ecosystems, including more complex wetlands and increases in the diversity of insects and birds (Chernov and Matveyeva 1997). The Intergovernmental Panel on Climate Change (IPCC) Fourth Assessment Report global climate models project future Arctic temperatures to warm from 2° to 9°C by 2100 (Chapman and Walsh

←

Figure 7. Regional time series of sea ice (blue), SWI (red), and NDVI for (a) the Northern Hemisphere, (b) Eurasia, and (c) North America from 1982 to 2008. Sea ice concentration (percent area; blue) is based on the climatological 50% concentration period. The percentage change for each variable from 1982 to 2008 is shown by the colored numbers, where trends significant at the 95% (90%) level or greater are in bold (italic). Small colored numbers shown in parentheses indicate the standard deviation of the linearly detrended time series.

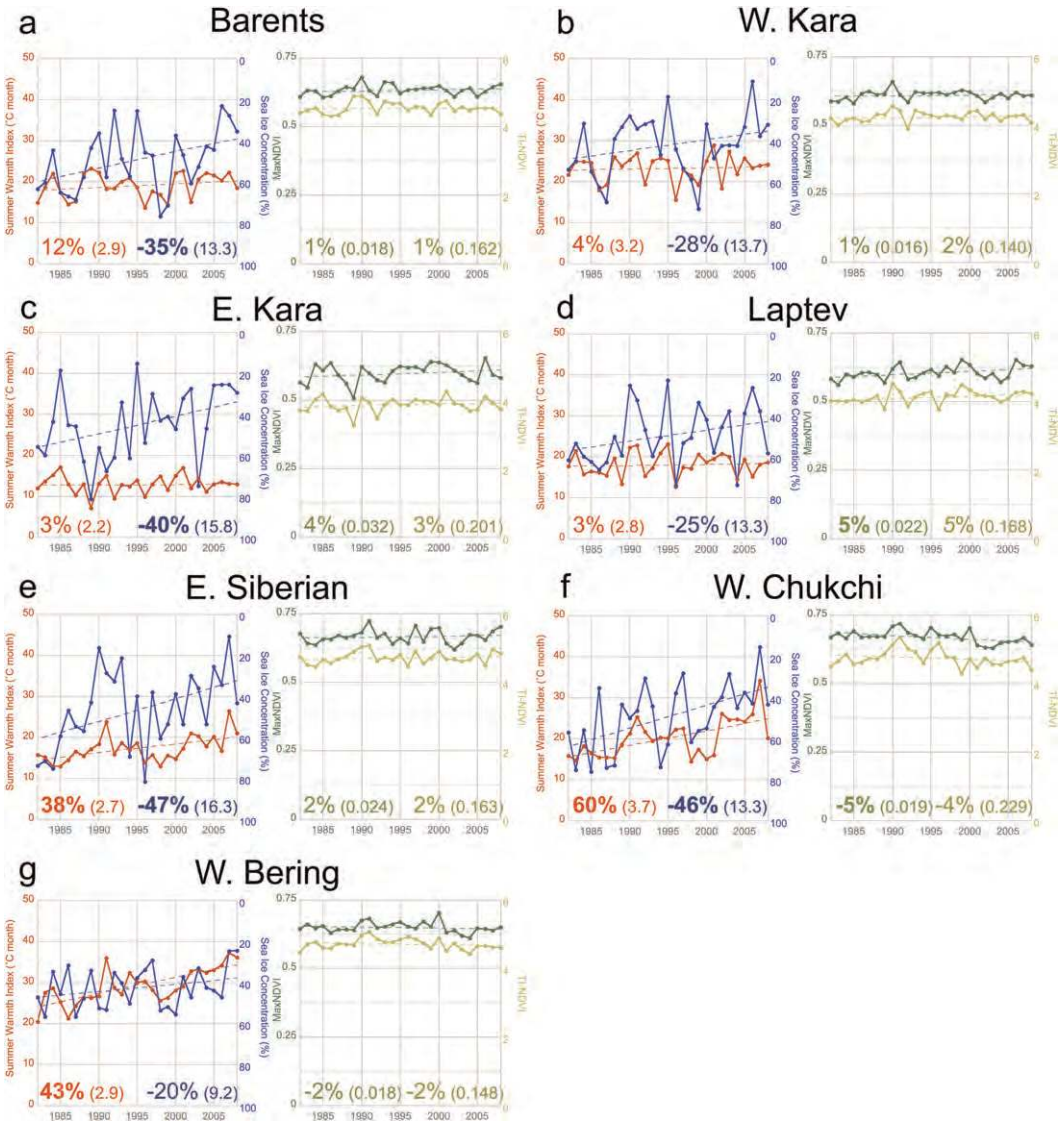

Figure 8. Regional time series of Eurasia, where the figure legend information is the same as in Figure 7.

2007). The changes in subzone A could be closer to the extreme temperature increases expected because of the shift at the coast from cold high-albedo ice to relatively warm low-albedo water. Although increases in biological diversity and increased productivity may be viewed positively in most parts of the world, these changes would essentially eliminate the unique character of this coldest bioclimate subzone.

The consistent correlations between springtime sea ice concentrations, summertime land warming, and tundra productivity support the conclusion that sea ice decreases are linked to warmer land temperatures and vegetation productivity increases. The correlations when combined with other evidence suggest, though not

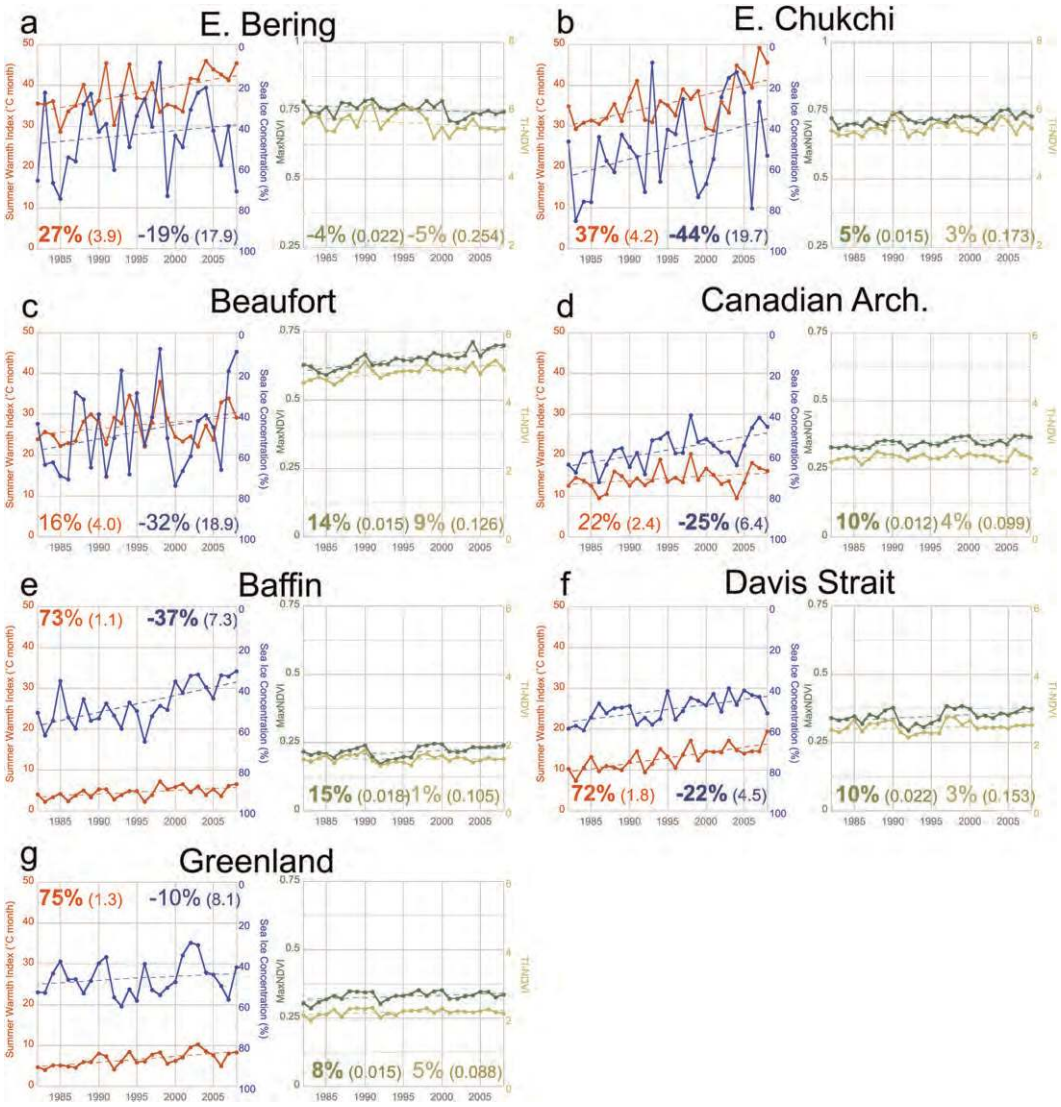

Figure 9. Regional time series of North America, where the figure legend information is the same as in Figure 7. East Bering and east Chukchi NDVI plots have a proportional but different *y* axis than the plots for other regions.

conclusively, that sea ice decline may be the primary driver of the near-coastal land surface warming. First, the general maritime nature of the Arctic tundra biome (Figure 1) indicates that average MaxNDVI and sea ice cover are closely linked, where areas with high (low) sea ice concentrations are adjacent to land with low (high) plant productivity, because summer warmth is limited because of nearby ice cover. Bekryaev et al. (Bekryaev et al. 2010) calculated annual average surface air temperature trends as function of distance from the Arctic coast (see their Figure 5) and found the largest trends occurred at maritime stations adjacent to the declining sea ice. In addition, global climate model studies with specified sea ice area, where

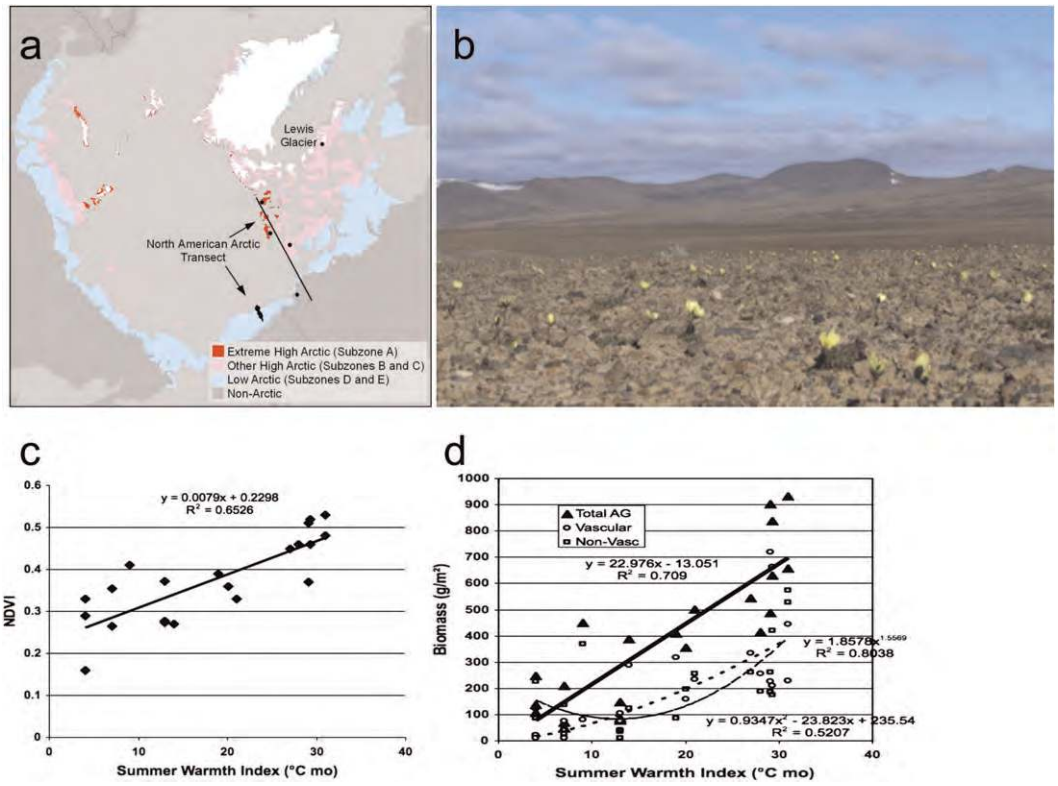

Figure 10. (a) Location of North American Arctic Transect (NAAT) and Lewis Glacier. Zonal boundaries follow the circumpolar Arctic vegetation map (Walker et al. 2005). (b) Typical subzone A zonal vegetation at Isachsen, Ellef Ringnes Island, Nunuvut, Canada, include scattered herbaceous species, such as *Papaver polaris* (yellow flowers), *Poa abbreviata*, and *Puccinellia* cf. *andersonii* (photo by D. A. Walker, 23 Jul 2005). (c) Relationship between NDVI (hand-held spectrometer) of zonal vegetation and summer warmth index along the NAAT. (d) Relationship between total above-ground, vascular, and nonvascular plant biomass with SWI along the NAAT (Walker et al. 2008). Data used in (c) and (d) are based on Epstein et al. (Epstein et al. 2008).

the atmospheric response is driven only by sea ice anomalies, indicate that either moderate (Bhatt et al. 2008) or large (Lawrence et al. 2008; Deser et al. 2010) reductions in near-coastal sea ice led to warmer air temperatures over the coastal Arctic. Deser et al. (Deser et al. 2010) compare a reduced fixed sea ice climate model experiment to a comparable fully coupled ice–ocean–atmosphere and found that sea ice loss accounts for most of the high-latitude warming in all seasons. Rennermalm et al. (Rennermalm et al. 2009) have argued that sea ice decline has led to ice sheet surface melt in Greenland in an observational study. Liu et al. (Liu et al. 2009) use remote sensing data from 1982 to 2004 in an attempt to separate surface temperature warming over the Arctic Ocean due to sea ice and that due to clouds (Liu et al. 2009). They found that the sea ice decline explained much of the

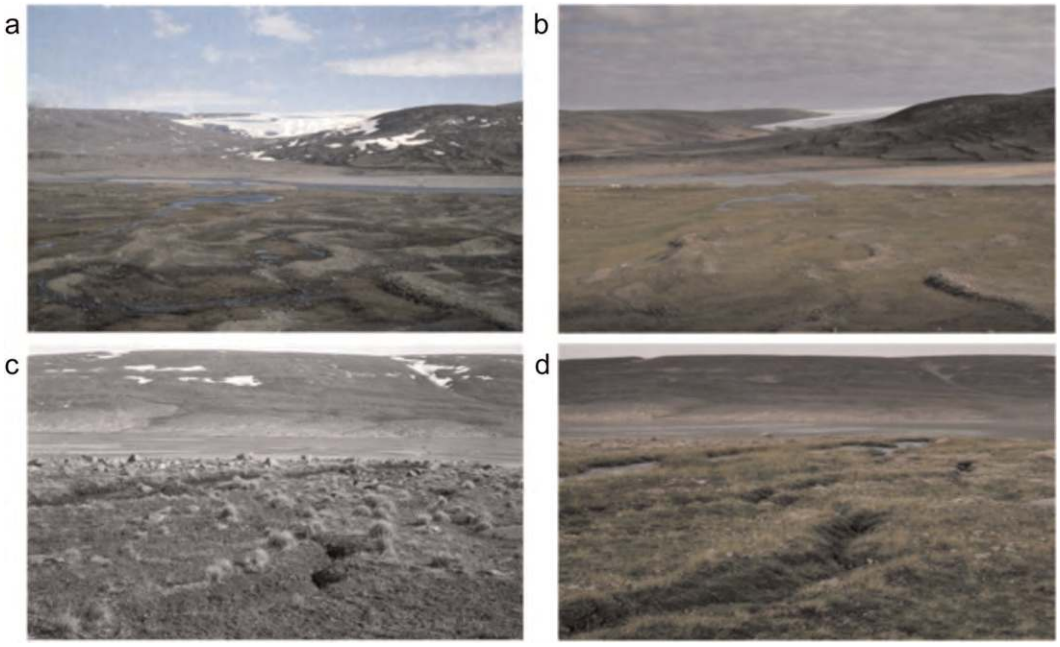

Figure 11. Repeat photography showing 46 years of change in recently deglaciated landscapes near the Lewis Glacier in north-central Baffin Island, Nunavut, Canada (see Figure 10 for location). (a),(b) Photos (70.397°N, 74.925°W) show an expansion and thickening of the plant cover on the cross-valley moraines in the foreground. In the background, the perennial snow banks vanished, the Lewis Glacier retreated up valley, and the level of the Barnes Ice Cap is noticeably lower on the horizon. The Lewis Glacier retreated 32 m yr^{-1} from 1964 to 2002 and 58 m yr^{-1} from 2002 to 2009. The landscape in the foreground is estimated to have been available for plant colonization between AD 1600 and 1700, when the Pintail Glacier, which blocked the Isortoq Valley, drained (Andrews and Webber 1969). (c),(d) Photos (70.3716°N, 75.0034°W) show vegetation change and loss of perennial snow banks in the Blockade Bend region of the Isortoq River near Cone Falls. This surface was deglaciated between AD 1550 and 1650 (Andrews and Webber 1969). Photos by (a) P. J. Webber, 10 Aug 1963; (b) C. Tweedie, 9 Aug 2009; (c) P. J. Webber, 9 Aug 1964; and (d) C. Tweedie, 6 Aug 2009.

fall warming in the Chukchi and Beaufort Seas, whereas clouds were the main driver of warming during spring. Although we suspect that sea ice decline significantly warms adjacent land areas, given the heterogeneity of the trends, seasonality of key processes, and complex nature of local circulations, further analysis is required to reach a firmer conclusion.

4. Conclusions

The previously documented changes of MaxNDVI in northern Alaska and the Beaufort Sea region are the largest in the Arctic (Figure 4) and are likely linked to

the strong retreat of sea ice in this region (Nghiem et al. 2007) and changes in erect shrub production (Tape et al. 2006; Lantz 2008). The corrected NDVI data north of 72°N permitted us to also document ecologically important percentage changes of NDVI in the High Arctic, where there are few or no shrubs. In these sparsely vegetated ecosystems, the NDVI changes are most likely a result of greater plant density. The vegetation change occurring in the vicinity of the Lewis Glacier is representative of similar changes all along the margins of the retreating glaciers in northern Canada and Greenland. Our conclusion is that the vegetation in the High Arctic is being affected by summer land-temperature increases that are likely associated with rapid sea ice declines and that areas marginal to perennial sea ice (subzone A) and the margins of the large glaciers will see the most rapid percentage changes if the perennial ice vanishes.

Acknowledgments. This study was supported by Grants NSF ARC-0531180, NASA NNG6NE00A, NSF ANS-0732885, NSF ARC-0902175; NASA Land Cover Land Use Change on the Yamal Peninsula; and a graduate fellowship (MKR) from the UAF Center for Global Change and the Cooperative Institute for Arctic Research (CIFAR) through the National Oceanic and Atmospheric Administration under Cooperative Agreement NA17RJ1224 with the University of Alaska.

This work benefited from insightful comments from two anonymous reviewers, Terry Chapin, and David Verbyla. H. Maier is thanked for the assistance with preparing graphics.

References

ACIA, 2004: *Impacts of a Warming Arctic: Arctic Climate Impact Assessment*. Cambridge University Press, 139 pp.

Alexandrova, V. D., 1980: *The Arctic and Antarctic: Their Division into Geobotanical Areas*. Cambridge University Press, 247 pp.

Andrews, J. T., and P. J. Webber, 1969: Lichenometry to evaluate changes in glacial mass budgets as illustrated from north-central Baffin Island, N.W.T. *Arct. Alp. Res.,* **1,** 181–194.

Bekryaev, R. V., I. V. Polyakov, and V. A. Alexeev, 2010: Role of polar amplification in long-term surface air temperature variations and modern Arctic warming. *J. Climate,* **23,** 3888–3906.

Bhatt, U. S., M. A. Alexander, C. Deser, J. E. Walsh, J. S. Miller, M. Timlin, J. D. Scott, and R. Tomas, 2008: The atmospheric response to realistic reduced summer Arctic sea ice anomalies. *Arctic Sea Ice Decline: Observations, Projections, Mechanisms, and Implications, Geophys. Monogr.,* Vol. 180, Amer. Geophys. Union, 91–110.

Bunn, A. G., S. J. Goetz, J. S. Kimball, and K. Zhang, 2007: Northern high-latitude ecosystems respond to climate change. *Eos, Trans. Amer. Geophys. Union,* **88,** , doi:10.1029/2007EO340001.

Chapman, W. L., and J. E. Walsh, 2007: Simulations of Arctic temperature and pressure by global coupled models. *J. Climate,* **20,** 609–632.

Chernov, Y. I., and N. V. Matveyeva, 1997: *Arctic Ecosystems in Russia*. *Polar and Alpine Tundra.* F. E. Wielgolaski, Ed., Elsevier, 361–507.

Comiso, J. C., 2003: Warming trends in the Arctic from clear sky satellite observations. *J. Climate,* **16,** 3498–3510.

——, and F. Nishio, 2008: Trends in the sea ice cover using enhanced and compatible AMSR-E, SSM/I, and SMMR data. *J. Geophys. Res.,* **113,** C02S07, doi:10.1029/2007JC004257.

——, C. L. Parkinson, R. Gersten, and L. Stock, 2008: Accelerated decline in the Arctic sea ice cover. *Geophys. Res. Lett.,* **35,** L01703, doi:10.1029/2007GL031972.

Deser, C., R. Tomas, M. Alexander, and D. Lawrence, 2010: The seasonal atmospheric response to projected Arctic sea ice loss in the late twenty-first century. *J. Climate,* **23,** 333–351.

Epstein, H. E., D. A. Walker, M. K. Raynolds, G. J. Jia, and A. M. Kelley, 2008: Phytomass patterns across a temperature gradient of the North American arctic tundra. *J. Geophys. Res.,* **113,** G03S02, doi:10.1029/2007JG000555.

Goetz, S. J., A. G. Bunn, G. J. Fiske, and R. A. Houghton, 2005: Satellite-observed photosynthetic trends across boreal North America associated with climate and fire disturbance. *Proc. Natl. Acad. Sci. USA,* **102,** 13 521–13 525.

Haugen, R. K., and J. Brown, 1980: Coastal-inland distributions of summer air temperature and precipitation in northern Alaska. *Arct. Alp. Res.,* **12,** 403–412.

Hudson, J. M. G., and G. H. R. Henry, 2009: Increased plant biomass in a High Arctic heath community from 1981 to 2008. *Ecology,* **90,** 2657–2663.

Jia, G. J., H. E. Epstein, and D. A. Walker, 2003: Greening of arctic Alaska, 1981–2001. *Geophys. Res. Lett.,* **30,** 2067, doi:10.1029/2003GL018268.

Kaufman, D. S., and Coauthors, 2009: Recent warming reverses long-term arctic cooling. *Science,* **325,** 1236–1239.

Kwok, R., and D. A. Rothrock, 2009: Decline in Arctic sea ice thickness from submarine and ICESat records: 1958–2008. *Geophys. Res. Lett.,* **36,** L15501, doi:10.1029/2009GL039035.

Lantz, T. C., 2008: Relative influence of temperature and disturbance on vegetation dynamics in the Low Arctic: An investigation at multiple scales. Ph.D. thesis, University of British Columbia, 167 pp.

Lawrence, D. M., A. G. Slater, R. A. Tomas, M. M. Holland, and C. Deser, 2008: Accelerated Arctic land warming and permafrost degradation during rapid sea ice loss. *Geophys. Res. Lett.,* **35,** L11506, doi:10.1029/2008GL033985.

Liu, Y., J. R. Key, and X. Wang, 2009: Influence of changes in sea ice concentration and cloud cover on recent Arctic surface temperature trends. *Geophys. Res. Lett.,* **36,** L20710, doi:10.1029/2009GL040708.

Myers, J. P., and F. A. Pitelka, 1979: Variations in summer temperature patterns near Barrow, Alaska: Analysis and ecological interpretation. *Arct. Alp. Res.,* **11,** 131–144.

Nghiem, S. V., I. G. Rigor, D. K. Petrovich, P. Clemente-Colón, J. W. Weatherly, and G. Neumann, 2007: Rapid reduction of Arctic perennial sea ice. *Geophys. Res. Lett.,* **34,** L19504, doi:10.1029/2007GL301138.

Post, E., and Coauthors, 2009: Ecological dynamics across the Arctic associated with recent climate change. *Science,* **325,** 1355–1358.

Raynolds, M. K., and D. A. Walker, 2009: Effects of deglaciation on circumpolar distribution of arctic vegetation. *Can. J. Remote Sens.,* **35,** 118–129.

——, J. C. Comiso, D. A. Walker, and D. Verbyla, 2008: Relationship between satellite-derived land surface temperatures, arctic vegetation types, and NDVI. *Remote Sens. Environ.,* **112,** 1884–1894.

Rennermalm, A. K., L. C. Smith, J. C. Stroeve, and V. W. Chu, 2009: Does sea ice influence Greenland ice sheet surface-melt? *Environ. Res. Lett.,* **4,** 024011, doi:10.1088/1748-9326/4/2/024011.

Rothrock, D. A., D. B. Percival, and M. Wensnahan, 2008: The decline in arctic sea-ice thickness: Separating the spatial, annual, and interannual variability in a quarter century of submarine data. *J. Geophys. Res.,* **113,** C05003, doi:10.1029/2007JC004252.

Rouse, W. R., 1991: Impacts of Hudson Bay on the terrestrial climate of the Hudson Bay lowlands. *Arct. Alp. Res.,* **23,** 24–30.

Serreze, M. C., M. M. Holland, and J. Stroeve, 2007: Perspectives on the Arctic's shrinking sea-ice cover. *Science,* **315,** 1533–1536.

Shippert, M. M., D. A. Walker, N. A. Auerbach, and B. E. Lewis, 1995: Biomass and leaf-area index maps derived from SPOT images for Toolik Lake and Imnavait Creek areas, Alaska. *Polar Rec.,* **31,** 147–154.

Stow, D. A., and Coauthors, 2004: Remote sensing of vegetation and land-cover change in arctic tundra ecosystems. *Remote Sens. Environ.,* **89,** 281–308.

Stroeve, J., M. Serreze, S. Drobot, S. Gearheard, M. Holland, J. Maslanik, W. Meier, and T. Scambos, 2008: Arctic sea ice extent plummets in 2007. *Eos, Trans. Amer. Geophys. Union,* **89,** doi:10.1029/2008EO020001.

Tape, K., M. Sturm, and C. Racine, 2006: The evidence for shrub expansion in Northern Alaska and the Pan-Arctic. *Global Change Biol.,* **12,** 686–702.

Treshnikov, A. F., 1985: *Atlas of the Arctic* (in Russian). Administrator of Geodesy and Cartography of the Soviet Ministry, 204 pp.

Tucker, C. J., and P. J. Sellers, 1986: Satellite remote sensing of primary production. *Int. J. Remote Sens.,* **7,** 1395–1416.

Verbyla, D., 2008: The greening and browning of Alaska based on 1982–2003 satellite data. *Global Ecol. Biogeogr.,* **17,** 547–555.

Walker, D. A., and Coauthors, 2003: Phytomass, LAI, and NDVI in northern Alaska: Relationships to summer warmth, soil pH, plant functional types, and extrapolation to the circumpolar Arctic. *J. Geophys. Res.,* **108,** 8169, doi:10.1029/2001JD000986.

——, and Coauthors, 2005: The Circumpolar Arctic Vegetation Map. *J. Veg. Sci.,* **16,** 267–282.

——, and Coauthors, 2008: Arctic patterned-ground ecosystems: a synthesis of field studies and models along a North American Arctic Transect. *J. Geophys. Res.,* **113,** G03S01, doi:10.1029/2007JG000504.

Webber, P. J., 1971: Gradient analysis of the vegetation around the Lewis Valley north-central Baffin Island, Northwest Territories, Canada. Ph.D. thesis, Queen's University, 366 pp.